Structure and Dynamics of Irreversible Single-Chain Nano-Particles in Dilute Solution. A Neutron Scattering Investigation

Marina González-Burgos,[†] Isabel Asenjo-Sanz,[†] José A. Pomposo,[‡,†] Aurel Radulescu,[¶] Oxana Ivanova,[¶,§] Stefano Pasini,[¶] Arantxa Arbe,[*,†] and Juan Colmenero[*,‡,†,‖]

[†]*Centro de Física de Materiales (CSIC, UPV/EHU) and Materials Physics Center MPC, Paseo Manuel de Lardizabal 5, E-20018 San Sebastián, Spain*

[‡]*Departamento de Física de Materiales (UPV/EHU), Apartado 1072, E-20080 San Sebastián, Spain*

[¶]*Jülich Centre for Neutron Science (JCNS) at Heinz Maier-Leibnitz Zentrum (MLZ), Forschungszentrum Jülich GmbH, Lichtenbergstraße 1, 85747 Garching, Germany*

[§]*Current address: GSI Helmholzzentrum für Schwerionenforschung GmbH, Planckstraβe 1, 64291 Darmstadt, Germany*

[‖]*Donostia International Physics Center (DIPC), Paseo Manuel de Lardizabal 4, E-20018 San Sebastián, Spain*

E-mail: a.arbe@ehu.eus; juan.colmenero@ehu.eus

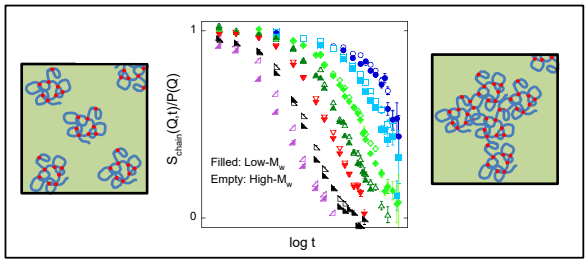
1
0
$S_{chain}(Q,t)/P(Q)$
Filled: Low-M_w
Empty: High-M_w
log t

Abstract

We present a small angle neutron scattering (SANS) and neutron spin echo (NSE) investigation on the structure and dynamics of irreversible single-chain nano-particles (SCNPs) in dilute solution. SCNPs are ultra-small soft nano-objects obtained by intramolecular folding / collapse of individual linear polymer chains (precursors). SANS has demonstrated the compaction of the macromolecules upon creation of internal cross-links, though their conformation is far from globular topology. To describe the dynamic structure factor of the SCNPs in solution we have taken into account their dual polymer / nano-particle character and applied theoretical approximations based on the Zimm model. The study reveals relaxation of internal degrees of freedom, but clearly slowed down with respect to the precursor counterparts. This effect is attributed to the internal friction associated to the compartmentation in domains within the macromolecule. We discuss the structural and dynamical similarities of SCNPs with disordered proteins, in particular with intrinsically disordered proteins. The high internal friction in both cases seems to be associated to the existence of internal domains.

Introduction

Single chain nano-particles (SCNPs) are synthesized by means of folding / collapse of individual polymer chains –called 'precursors'– by means of intramolecular bonding (i.e., covalent, non-covalent or reversible covalent bonds). Interesting properties with potential applications in different fields have been identified for SCNPs, like sensing, catalytic or controlled drug delivery capabilities,[1–10] rendering them as promising elements in nano-technology (see, e. g.,[5–9,11–15]). Nowadays it is known that the usual techniques for SCNP formation in good solvent conditions result in sparse, non-globular morphologies in solution, even by employing highly-efficient intra-chain cross-linking techniques (e. g., 'click' chemistry) or supramolecular interactions.[16] On the other hand, the dynamical behavior of SCNPs is of great importance in order to determine their possible applications, since their internal mobility is the one responsible for many of their unique capabilities. Unraveling the actual structure and dynamics of SCNPs in solution and, hence, establishing reliable structure-properties relationships, is obviously at the basis of a rational design of SCNPs with tailor-made properties. To decipher the conformation and dynamic behavior of these nano-objects, scattering techniques are obviously the right choice. Small angle (neutron or X-ray) scattering and neutron spin echo (NSE) experiments are particularly well suited for this task. They provide microscopic insight into, respectively, the form factor and the dynamic structure factor, at length scales where the internal macromolecular properties are revealed. The application of small angle scattering allowed, in fact, establishing the above mentioned scarce compaction degree for SCNPs suggested by dynamic light scattering (DLS) and/or size exclusion chromatography (SEC) measurements. Regarding the dynamics, up to date the NSE investigations of SCNPs in solution have been restricted to the case of reversible SCNPs.[17] In that work, the relevance of internal friction in the dynamics of the collapsed macromolecules was put forward.

In addition to their technological potential, SCNPs also have high interest from a basic point of view. In particular, it was suggested the possibility of considering them as a *simplified* model for investigating the folding process of proteins –though of course some pe-

culiarities of protein folding as e. g. small folding times and possibly two-state folding would not be reproduced by the folding / collapse process leading to nano-particle formation. Interestingly enough, the obtained degrees of compaction of synthetic SCNPs are similar to those displayed by disordered proteins, in particular by intrinsically disordered proteins (IDPs).[18] Nowadays we know that these bio-macromolecules are ubiquitous in nature and responsible of functions of utmost relevance in biological systems.[19] The functionality of IDPs emanates from their internal dynamics and flexibility, which enable them to respond quickly to environmental changes and to bind with different cellular targets. Noteworthy, the microscopic insight provided by NSE on the internal dynamics of IDPs revealed a strong impact of internal friction –also in common with the only existing result on SCNPs above mentioned.[17] In this direction we note that, recently, the outstanding properties of some antimicrobial polypeptides and both the size and function of certain metalloproteins, intrinsically disordered as well as structured proteins have been mimicked with SCNPs.[20–25]

In this work, we report on a small angle neutron scattering (SANS) and NSE investigation of the conformation and dynamics of irreversible SCNPs in dilute solution. The SCNPs are obtained from poly(methyl methacrylate) (PMMA)-based precursors, using a synthesis protocol that results in covalent bridges among different functionalized monomers along the chain. Two molecular weights have been investigated. We first address the structural properties of the macromolecules in dilute solution, corroborating also in these systems the finding of sparse morphologies. At the concentration investigated by NSE, the SANS experiments allow determining the structure factor relating the centers of mass of the macromolecules. The interferences among different SCNPs lead to a markedly different structure factor with respect to that of the linear counterparts. A broad but well defined peak arises as signature of the particle-character imprinted by internal cross-links. Knowledge about the structure factor is also indispensable to derive the scattering vector dependent translational diffusion coefficient starting from DLS results.

The NSE results are presented in the second part of the paper, where we face the dynam-

ical aspects. First, the lower molecular weight sample is considered, in comparison with the corresponding linear precursor as reference. After a phenomenological analysis in terms of stretched exponentials, the internal modes contribution to the single chain dynamic structure factor is obtained considering the input of the translational diffusion above mentioned. The intramolecular contribution to the dynamics is still remarkable, reflecting the internal flexibility of the macromolecules. Three versions of the Zimm model (the original one, a modified version considering a limited number of contributing modes and one, which takes into account the internal friction) are considered as possible simplified theoretical frameworks. The impact of internal friction affecting the short-wavelength modes is easily recognizable in the dynamics of SCNPs and can be correlated with the degree of compaction. Still, some long-wavelength modes are active in the internally cross-linked chains. Structural and dynamical analogies between our SCNPs and disordered proteins are discussed, putting forward the role played by the internal domains characterizing both kinds of macromolecules.

Experimental

Samples

We investigated SCNPs obtained through Michael addition-mediated multidirectional self-assembly.[26] Trimethylolpropane triacrylate (Sigma-Aldrich, technical grade) acted as intrachain cross-linking agent. Precursors were random copolymers of methyl methacrylate (MMA) and (2-acetoacetoxy)ethyl methacrylate (AEMA).

The synthesis of low-molecular weight (M_w) precursors was carried out as follows: In a typical procedure, MMA (1mL, 9.4mmol), AEMA (0.6mL, 3.1mmol), 2-cyanoprop-2-yl-dithiobenzoate (CPDB) (6.9mg, 3.12×10^{-2}mmol) and 2,2-azobis(2-methylpropionitrile) (AIBN) (1.3mg, 7.8×10^{-2}mmol) were dissolved in ethyl acetate (1.6mL). The reaction mixture was degassed by passing argon for 15 min. The copolymerization reaction was carried out at 65°C for 18h. The resulting precursor was isolated by precipitation in methanol and

further drying under vacuum. The resulting copolymer had composition (H^1 NMR) = 28.4% AEMA. For the synthesis of the high-M_w precursor, the same conditions were applied with exception of the amounts of CPDB (1.4mg, 6.24×10^{-3}mmol), AIBN (1mg, 6.24×10^{-3}mmol) and ethyl acetate (3.12mL). The resulting copolymer had composition (H^1 NMR) = 30.1% AEMA. Molecular weights and polydispersities of the precursors (as determined by SEC) are shown in Table 1.

In a typical reaction for the synthesis of low-M_w NPs low-molecular weight precursor (150mg, 0.31mmol), multifunctional cross-linker (Trimethylolpropane triacrylate, TMT, 28.2mg, 0.10mmol) and catalyst (KOH, 8.9mg, 0.16mmol) were dissolved in tetrahydrofuran (THF, Scharlab) (150mL) at room temperature (see Fig. 1). The progressive folding/collapse process was followed through simultaneous SEC/MALLS measurements. After reaction completion (3 days), a few drops of hydrochloric acid were added to deactivate the catalyst, the mixture was concentrated and the SCNPs were isolated by precipitation in diethyl ether and further drying under vacuum. For the synthesis of high-M_w NPs, the same procedure was carried out using 30.1mg, 0.11mmol of TMT, 9.4mg, 0.17mmol of KOH and 150mg, 0.34mmol of the corresponding precursor.

In the solutions investigated by neutron scattering, deuterated N,N-dimethyl formamide (dDMF, 99.5 atom% D, from Acros Organics) was used as solvent.

Table 1: Parameters characterizing the molecular weight and form factor of the precursors and SCNPs in solutions at 2 mg/mL obtained from fits of generalized Gaussian functions (Eq. 4), and values of the overlap concentration $c^\star$

M_w^{Prec} (g/mol)	PDI^{Prec}	$\overline{R}_g^{Prec}$ (nm)	ν^{Prec} (g/L)	$c^\star_{Prec}$ (nm)	$\overline{R}_g^{NP}$	ν^{NP} (g/L)	$c^\star_{NP}$
52540	1.03	7.3	0.59	54	5.9	0.52	103
272100	1.4	16.5	0.59	24	9.3	0.46	134

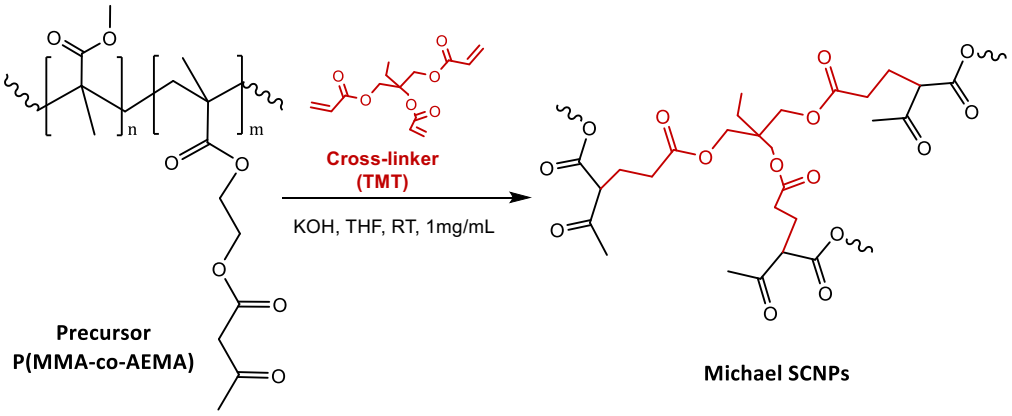

Figure 1: Scheme of the Michael synthesis route followed in this work for the formation of the SCNPs.

Scattering Experiments

Small Angle Neutron Scattering

The accessed magnitude in a diffraction experiment is the differential scattering cross section $d\sigma/d\Omega$, i. e., the probability of a particle of the incident beam being scattered out into the solid angle $d\Omega$. The scattering vector (Q)-value is determined as $Q = 4\pi \sin(\theta)/\lambda$, θ being half of the scattering angle and λ the wavelength of the incident probe particle. The differential cross section measured by neutrons contains a Q-independent incoherent term and a coherent term originated by the interference of scattered waves at different nuclei. The coherent contribution thus contains the information on the structural features of the sample. For a monodisperse collection of spherically symmetric particles, the coherent scattering

cross section is given by

$$\left(\frac{d\Sigma(Q)}{d\Omega}\right)_{coh} = \phi\Delta\rho^2 V^2 P(Q) S_{CM}(Q) \tag{1}$$

where ϕ is the volume fraction, $\Delta\rho$ is the difference in scattering length density between the particles and the solvent or the matrix, V is the volume of the particle, $P(Q)$ is the form factor of the particles and $S_{CM}(Q)$ is the structure factor of their centers of mass. For neutrons, the scattering length depends in a non-systematic way on the atomic mass. In particular, the huge difference between the scattering length of deuterons and hydrogens provides a nice way to increase the scattering contrast –and thereby the measured intensity– between the components in a mixture (see e.g. Refs.[27–30]).

The Small Angle Neutron Scattering (SANS) experiments were performed on the instrument KWS-2 at the Forschungs-Neutronenquelle Heinz Maier-Leibnitz (MLZ) in Garching[31] with $\lambda = 5.27$ Å and using sample-detector distances (SDD) of 1.15 and 5.76 m. For the high-M_w-sample, SDD=19.76 m was also employed. The solutions in dDMF (concentrations of 2, 4, 8 and 25mg/mL) were filled in 2 mm thick Hellma Quarz cells, placed in transmission geometry. Experiments were carried out at room temperature. The azimuthally averaged scattered intensities were obtained as function of Q. The signal from the solvent was measured under the same conditions and properly subtracted from the measurements on the solutions. The Q-independent incoherent contribution was estimated to be at most 7×10^{-3} cm^{-1} (for the highest concentration). It was also subtracted from the results as a constant background. Thus, the results shown correspond directly to the coherent cross-section.

Neutron Spin Echo

The kinetic energies of neutrons –in the range of the meV– are comparable with the excitation energies of atomic or molecular motions. Slow relaxational motions can be detected by

a velocity change of the neutron. From the so-called quasielastic neutron scattering experiments exploiting this capability, information about the time-dependent atomic positions can be obtained.

The Neutron Spin Echo (NSE) technique provides the highest resolution achievable by neutron scattering methods. This technique presents in addition two big advantages: (i) it delivers the information directly in the time domain, allowing for a deconvolution of the experimental results from resolution effects by simple division and (ii) the measuring procedure strongly suppresses incoherent contributions. In isotopically labeled samples, like those investigated in this work (protonated solute macromolecules in deuterated solvent), and in the explored low Q-range, NSE results provide the time evolution of the correlations between pairs of atoms belonging to a labelled macromolecule. The delivered magnitude is the normalized single chain dynamic structure factor:

$$NSE(Q,t) = \frac{S_{chain}(Q,t)}{P(Q)}. \tag{2}$$

The denominator is the above introduced form factor $P(Q)$ –the $t = 0$ limit of the single chain dynamic structure factor $S_{chain}(Q,t)$ (see e. g. Refs.[32–34]).

NSE experiments were performed at 300 K using the J-NSE instrument also at the MLZ.[35] Combining two wavelengths (8 and 12 Å), Fourier times in the range $0.1 \leq t \leq 140$ ns were covered in the Q-range: $0.03 \leq Q \leq 0.2$ Å^{-1}. Solutions of low-M_w and High-M_w NPs in dDMF at 25 mg/mL concentration were investigated. This relatively high concentration was chosen in order to produce a sufficiently strong NSE signal, being still well below the overlap concentration [$c^\star = M_w/(4/3\pi\overline{R}_g^3 N_A)$, see Table 1]. The equivalent solution of low-M_w precursor macromolecules was also studied as reference. The data were corrected for the solvent contribution by subtracting the background signal measured on the solvent.

Dynamic Light Scattering

From Dynamic Light Scattering (DLS) experiments the diffusion coefficients were determined. The scattering vector Q is then given by $Q = 4\pi n_d \sin\theta/\lambda_o$, with λ_o the wavelength in vacuum and n_d the refractive index. The experiments were performed on a Malvern Zetasizer Nano ZS apparatus at 298 K. Solutions in DMF with the same concentration as the NSE samples (25 mg/mL) were investigated. This equipment does not allow correction for multiple scattering effects, as it is the case of instruments including the 3D-modulation technology. However, at the concentration studied we do not expect these effects to be important. At the experimental conditions employed [2θ=173°, λ_o=633 nm, n_d(DMF)=1.431], the Q-value explored was 0.00284Å^{-1}.

Structural Characterization

The SANS results on the solutions of SCNPs are compared with those on the corresponding linear precursor system in Figs. 2(a) and (b). The concentration is 2 mg/mL, i. e., well below the overlap concentration in all cases (see Table 1) and there are thus no position-position correlations between the different macromolecules. Consequently, the structure factor of the centers of mass $S_{CM}(Q)$ in Eq. 1, describing the interference of scattering from different particles, can be considered as 1 to a good approximation, yielding

$$\left(\frac{d\Sigma(Q)}{d\Omega}\right)_{coh} \approx \phi\Delta\rho^2 V^2 P(Q). \tag{3}$$

The Q-dependence of the measured curves is thus entirely determined by the form factor of the dissolved particles $P(Q)$. A clear decrease of the macromolecular size is observed upon cross-linking. For the case of the high-M_w macromolecules, this is directly evidenced in the Guinier representation shown in Fig. 2(a). From Guinier fits [$\left(\frac{d\Sigma(Q)}{d\Omega}\right) \propto \exp -Q^2R_g^2/3$] in the proper Q-regime ($Q < 1/R_g$), a reduction of the radius of gyration R_g from 14 nm to 9 nm

is obtained for these large chains. Additional information can be obtained from the slope of the intensity at higher Qs, in the intermediate (fractal) regime, that directly reveals the scaling exponent ν relating mass and size of the macromolecule. In this Q-regime the form factor namely scales as $P(Q) \sim Q^{-1/\nu}$.[29,36] The curves in Fig. 2(b) show that the slope of the intensity increases from the linear case to the SCNPs. The scaling exponent obtained for the precursor is that expected for linear chains in good solvent (Flory exponent, $\nu_F \approx 0.59$), which conformation follows a self-avoiding path. Lower values of ν reflect a compaction of the chain. For the NPs, a scaling exponent close to 0.50 is obtained. The scaling exponent 0.5 corresponds to a linear chain in θ-solvent conditions, describing a random walk in space. The highest degree of compaction achieved in an equilibrium globule is reflected in a ν-exponent of 1/3 (fractal dimension $D = 3$).[36,37]

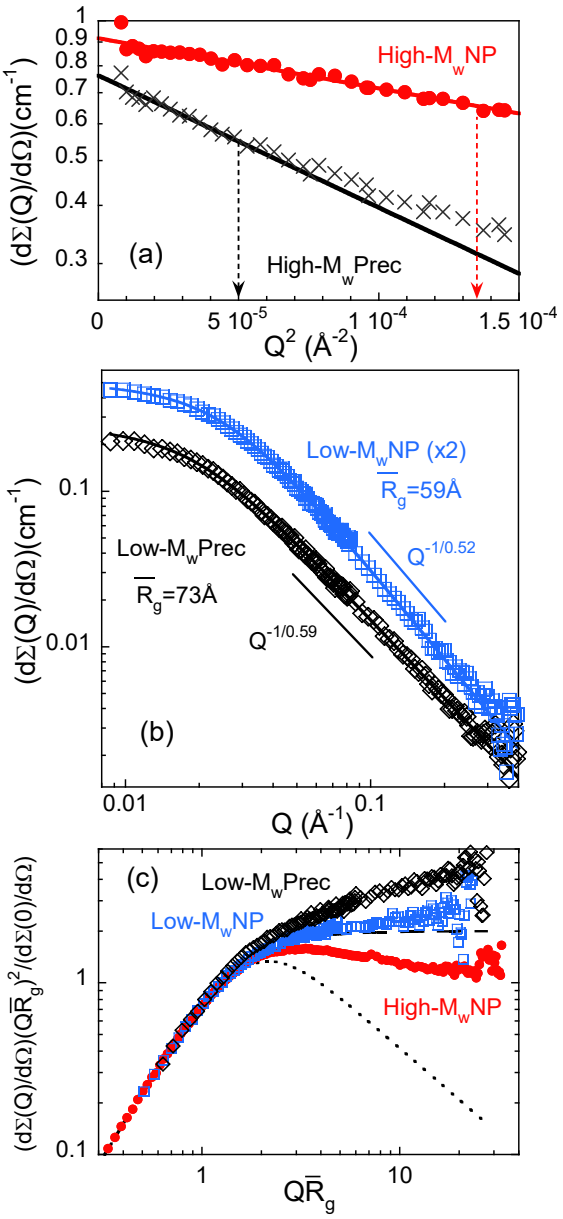

Figure 2: (a) Guinier representation of the SANS results on the high-M_w macromolecules: precursors (black crosses) and SCNPs (red circles). Solid lines are fits in the Guinier regime, which limit $1/R_g^2$ is depicted in each case by the corresponding vertical arrow. (b) SANS results on the low-M_w precursor (black diamonds) and the SCNPs obtained from it (blue squares). The latter have been multiplied by 2 for clarity. The solid lines are fits of Eq. 3 with generalized Gaussian coil form factors (Eq. 4) for $P(Q)$. (c) Kratky representation of the results on the SCNPs and the low-M_w precursors with the same symbol code as used in panels (a) and (b). The cases of a random coil (ν=0.5, dashed line) and a compact globule (ν=1/3, dotted line) are shown for comparison. In all cases the concentration is 2 mg/mL.

To obtain accurate values for the scaling exponent and size dimensions, the experimental form factors were described by generalized Gaussian coil functions[38]

$$P(Q) = \frac{1}{\nu U^{\frac{1}{2\nu}}}\gamma\left(\frac{1}{2\nu}, U\right) - \frac{1}{\nu U^{\frac{1}{\nu}}}\gamma\left(\frac{1}{\nu}, U\right) \tag{4}$$

[$U = (2\nu+1)(2\nu+2)Q^2\overline{R}_g^2/6$; $\gamma(a,x) = \int_0^x t^{a-1}\exp(-t)\mathrm{d}t$]. The such deduced values of ν and $\overline{R}_g = \sqrt{\langle R_g^2\rangle}$ are listed in Table 1 for the highest dilution case. The corresponding average end-to-end distance can be calculated as[39]

$$\overline{R}_e = \sqrt{(2\nu+1)(2\nu+2)}\overline{R}_g. \tag{5}$$

As can be seen in Fig. 2(b), the fitting curves are practically indistinguishable from the experimental data. The compaction is more efficient for the higher molecular weight, where the value of the scaling exponent decreases to 0.46; however, even in this case the achieved conformation is still far from the globular one (ν=1/3). This is illustrated in the Kratky representation of Fig. 2(c). Though the high-M_w SCNPs present a maximum in this kind of plot, it is not as pronounced as that expected for a globular object and resembles more the situation of a random coil.

As it has been commented in the Introduction, the analysis of size data from the literature obtained by SEC and/or DLS for a large number of SCNPs in solution, covering from covalent to non-covalent bonded SCNPs synthesized in good solvents shows that, in general, current synthesis techniques yield open, sparse morphologies characterized by scaling exponents $\nu \approx 0.5$.[40] This range of scaling exponents is also that found for the form factor of intrinsically disordered proteins (IDPs);[18,41–44] thus, both nano-objects display similarly open conformations instead of globular ones. The underlying physical mechanism leading to such morphologies of the SCNPs was elucidated by molecular dynamics (MD) simulations.[16] Under the good solvent conditions during the synthesis of SCNPs (imposed to avoid unwanted intermolecular cross-linking events), the linear precursors universally adopt self-

avoiding conformations.[37] Such conformations mostly favor bonding of reactive groups that are separated by short contour distances. This mechanism promotes local globulation along the chain. On the contrary, long-range loops efficient for global, large-scale chain compaction are highly infrequent.[16]

MD-simulations have also shown that SCNPs, as IDPs, present locally compact regions –called 'domains'– of the chain connected by more flexible disordered segments.[45] A domain in a SCNPs is defined as a cluster of rings, where the criterion for clustering is having monomers in common. An illustrative example is shown in Fig. 3, which includes snapshots of two simulated SCNPs in dilute conditions.[45] There, different domains are depicted in different colors. Some monomers do not belong to any domain, forming flexible segments connecting domains. As can be seen in this figure, the domain size is broadly distributed –even within each SCNP. It can vary from a few monomers to essentially the whole macromolecule. A statistical analysis of the simulation results shows that most of the domains are small, as a consequence of the above mentioned self-avoiding character of the precursor chain. This leads to the formation of a large fraction of small rings that do not even share monomers with other rings in the macromolecule.

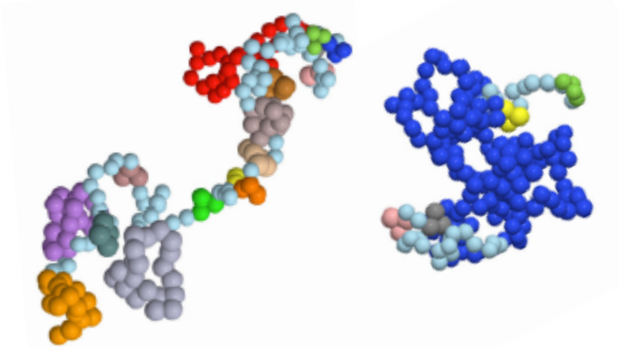

Figure 3: Snapshots of two simulated SCNPs in dilute conditions.[45] Different colors represent different domains. Beads in light blue represent monomers not belonging to any domain.

Since the NSE experiments were carried out on solutions with a higher concentration, we explored the concentration dependence of the structural properties in the solutions. According to Eq. 1, if the form factor of the particles $P(Q)$ is not affected by crowding, representing the measured intensities divided by the corresponding concentration should lead to a master curve in absence of interactions between the nano-objects. We shall call this normalized magnitude $i(Q,c)$, $i(Q,c) \equiv (d\Sigma/d\Omega)_{coh}(Q,c)/c$. The results obtained for the SCNPs are shown in Fig. 4. The data collapse rather well in a single curve for concentrations up to 8 mg/mL, but those obtained at 25 mg/mL clearly do not overlap with this curve in the low-Q range.

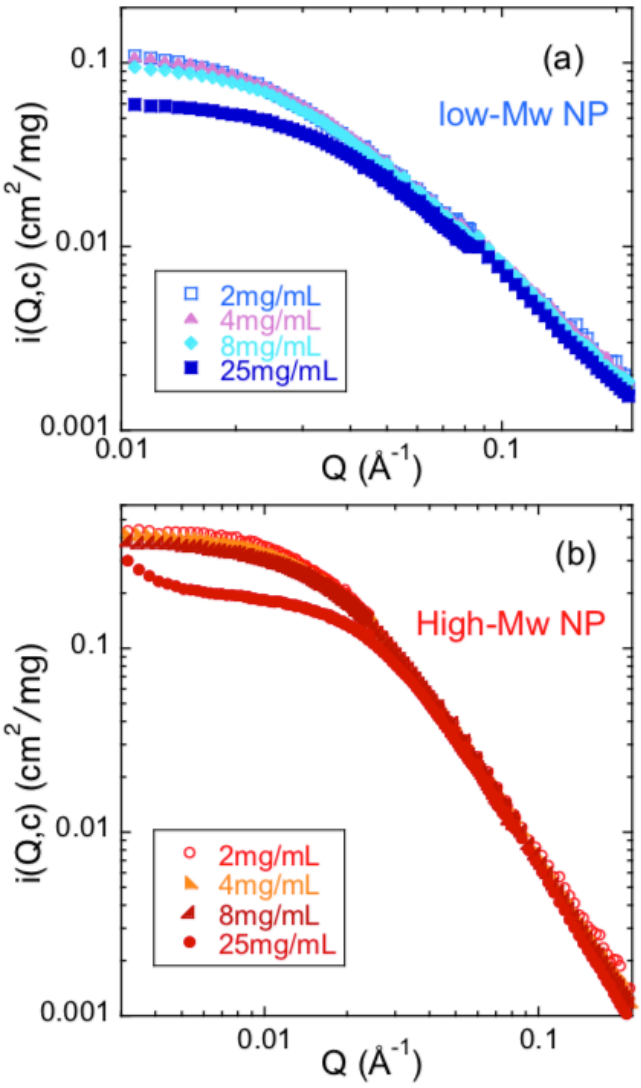

Figure 4: SANS intensity measured at different concentrations, divided by the corresponding concentration value, for (a) low-M_w SCNPs and (b) high-M_w SCNPs.

The effect of crowding on the conformation of SCNPs has been thorouhgly investigated by SANS and DLS[46,47] as well as by MD-simulations.[45] The simulations showed that the form factor of SCNPs remains unaffected for concentrations below $c^\star$. Above this concentration, the macromolecules continuously become more and more compact, and their conformations approach those of crumpled globular objects for bulk densities. These results could be confirmed by experiments on PMMA-based SCNPs –similar to those here investigated–, when the environment of the SCNPs was crowded by adding inert linear polymeric chains.[46] When crowding was induced by increasing the concentration of SCNPs, aggregation effects became important, preventing drawing conclusions about the conformation of SCNPs not belonging to the agglomerates. This aggregation started to be noticed above a threshold concentration about $c^\star/3$. Thus, according to those works, in the concentration range here explored –including the concentration chosen for the NSE experiments– we would not expect a change in the form factor of the SCNPs with respect to that observed in the infinite dilution limit. The different shape of the intensity at 25 mg/mL with respect to the high dilution cases would be due to non-negligible interactions between the macromolecules –the structure factor of the centers of mass $S_{CM}(Q)$ deviates from unity.

The knowledge of $S_{CM}(Q)$ is a prerequisite for the analysis of the NSE dynamics results we present in the following section, since it allows determining the Q-dependent translational diffusion coefficient $D_{CM}(Q)$ (see below). Under the hypothesis of unperturbed form factor[45,46] and assuming the validity of Eq. 1 for our solutions, the structure factor of the centers of mass at a given concentration c, $S_{CM}(Q,c)$, can be calculated as $S_{CM}(Q,c) = Ai(Q,c)/i(Q,c_0)$. Here, c_0 is a concentration low enough to assure that the scattered intensity exclusively reflects the unperturbed form factor of the macromolecules (e. g. 2 or 4 mg/mL) and $A \approx 1$ is a scaling correction factor to obtain the proper asymptotic limit of 1 at high-Q values. We recall that this approach is the best estimate we can do with our experimental data and based on the above assumptions, and therefore the resulting functions can be considered as 'effective' structure factors. They are shown in Fig. 5(a) for both kinds of SCNPs, and

the low-M_w precursor. Intramolecular cross-linking has a noticeable impact on $S_{CM}(Q)$. While for the linear chains the structure factor shows an increase up to $Q \approx 0.06\text{Å}^{-1}$ with little variation around 1 at higher Qs, $S_{CM}(Q)$ of the corresponding SCNPs displays a clear –though broad– peak, indicating broadly distributed inter-particle distances. The maximum is centered at lower Q-values in the case of the high-M_w NPs, corresponding to larger average separations between the NPs. Since the same total polymeric mass in the system is distributed among about five-fold less nano-objects in the bigger macromolecules with respect to the smaller ones, they are expected to be more separated in average from each other. We can also observe still a rather high value of $S_{CM}(Q)$ in the asymptotic $Q \to 0$ limit, indicative for a large compressibility of the systems. For the precursor, we have included the prediction of the classical random phase approximation $S_{RPA}(Q) = [1 + \beta P(Q)]^{-1}$ [27] with $P(Q)$ the chain form factor describing the results at high dilution. The parameter β is related to the strength of the interaction potential (we used β=0.76). Clear deviations are observed, demanding more complex approaches as e. g. that proposed in Ref. [48] and applied in polystyrene solutions [27,49] or the Gaussian core model. [50] We note that for the SCNPs, the hard-sphere model fails to reproduce the experimental data. The description of the structure factors of these nano-objects is beyond the scope of this work and shall be subject of future studies involving MD-simulations. In order to calculate the values of $D_{CM}(Q)$, we used the smoothed solid lines describing the corresponding structure factors in Fig. 5(a). The such obtained values of $D_{CM}(Q)$ are shown in Fig. 5(b).

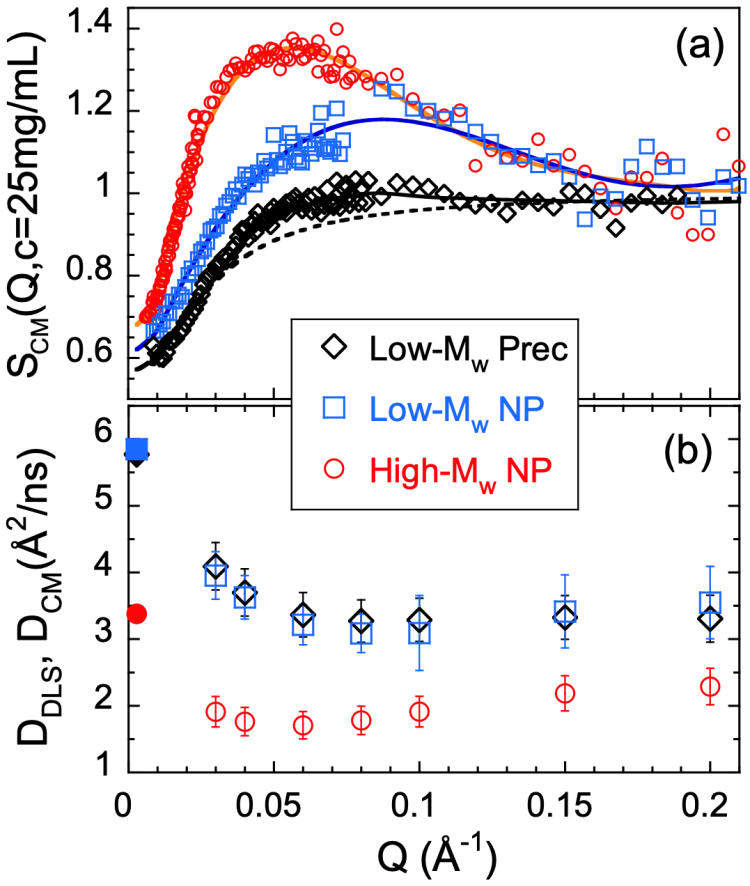

Figure 5: (a) Static structure factor of the centers of mass deduced from the SANS measurements at 25 mg/mL. Squares correspond to low-M_w SCNPs, circles to high-M_w SCNPs and diamonds to low-M_w-precursors. The values of A used were 1.15 for precursors, 1.2 for low-M_w and 1.4 for high-M_w. Solid lines are smoothing functions. For the precursor, the dotted line shows the classical RPA prediction. (b) Translational diffusion coefficient calculated by Eq. 8 for the Q-values investigated by NSE (empty symbols) using the values obtained from DLS at 25 mg/mL (Q=0.00284Å^{-1}) (solid symbols).

Dynamics

Phenomenological Approach

Figure 6 directly compares the NSE results obtained on the solutions of the low-M_w macromolecules, prior and after internal cross-linking. For all the Q-values investigated by NSE the decay of the dynamic structure factor of the precursor chains is more pronounced than that of the SCNPs. Before providing a quantitative analysis of the data in terms of existing theoretical frameworks for polymer dynamics, we present a simple phenomenological approach to describe the dynamic results on the low-M_w systems. It shall serve as a first scrutiny of the impact of internal cross-links on the dynamics and provide a rough idea about the nature of the contributions at the different length scales explored. The approach consists of using stretched exponential functions

$$\frac{S_{chain}(Q,t)}{P(Q)} = \exp\left[-\left(\frac{t}{\tau_w}\right)^{\beta_w}\right] \tag{6}$$

characterized by the relaxation time τ_w and the stretching exponent β_w. In the case of simple diffusion, there is no deviation from a single exponential (β_w=1), and τ_w is related with the diffusion coefficient D as $\tau_w = D^{-1}Q^{-2}$. The stretched exponential function reproduces rather well the data (see Fig. 6), with the values of τ_w and β_w shown in Fig. 7(a) and (b). As can be seen in this figure, the Q-dependence of τ_w and the values of β_w differ from the case of a simple diffusion, indicating additional contributions with respect to just translational motion of the whole macromolecule. Thus, internal degrees of freedom also contribute to the dynamic structure factor at the length scales probed by NSE. To compare results from the two samples and at different Q-values, we have taken into account the differences in the shape parameters, calculating the average time corresponding to each Q-value $\langle\tau\rangle = \tau_w\Gamma(1/\beta_w)/\beta_w$. From this magnitude, we have defined an 'effective diffusion coefficient' $D_{eff}(Q)$ as $D_{eff}(Q) = \langle\tau\rangle^{-1}Q^{-2}$. The results are represented in Fig. 7(c). $D_{eff}(Q)$ is

systematically smaller for the SCNPs than for the linear precursors. The difference seems to be amplified with increasing Q-value. Thus, the NSE experiments evidence a slowing down of the dynamics upon internal cross-linking of the macromolecules, which becomes more dramatic when the length scale of observation decreases (at higher Q-values).

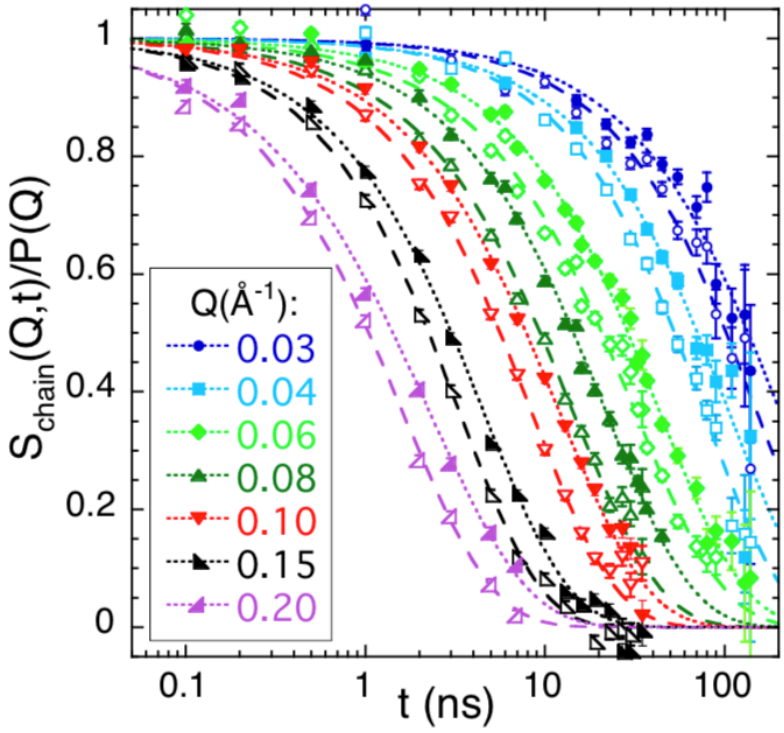

Figure 6: NSE results on the low-M_w SCNPs (filled symbols) and the corresponding precursor (empty symbols) solutions at the different Q-values indicated. Lines are fits of stretched exponentials to the data.

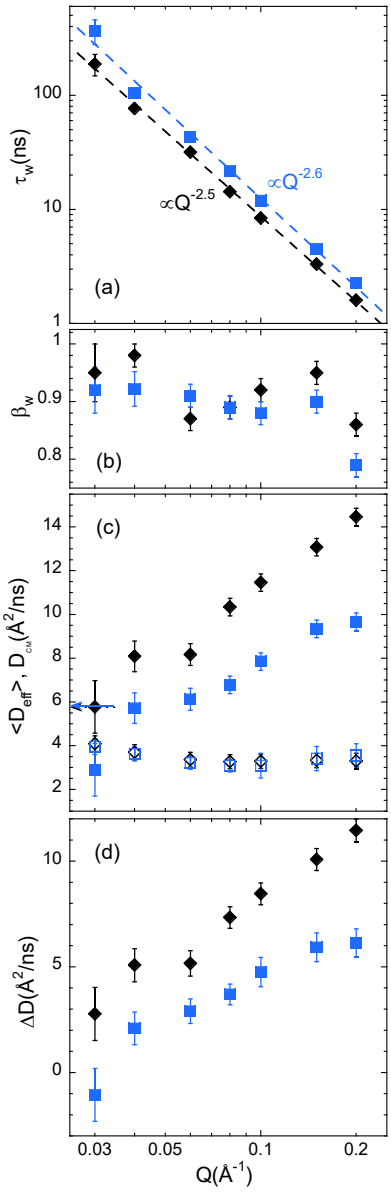

Figure 7: Scattering vector dependence of the parameters involved in the phenomenological approach for the low-M_w precursors (filled diamonds) and SCNPs (filled squares) in solution: (a) characteristic time; (b) stretching exponent; (c) effective diffusion coefficient D_{eff} and (d) difference between D_{eff} and the translational diffusion coefficients. The latter are shown in (c) by the corresponding empty symbols. Lines in (a) are fits of power laws with exponents as indicated. Arrows in (c) mark the values of D_{DLS} for SCNPs (solid) and precursor (dotted). They are almost indistinguishable.

In Fig. 7(c) the arrows mark the values of the diffusion coefficient determined at a much smaller scattering vector from the DLS experiments, D_{DLS}. In the Guinier regime explored by DLS, the macromolecules can be considered as 'point-like' particles undergoing Brownian motion. Thus, the diffusion coefficient obtained is that corresponding to the center-of-mass translation. The values were 5.77 and 5.85 Å^2/ns for precursor and SCNPs, respectively. Internal cross-links induce a slight increase of the value of D_{DLS}, as it would be expected from a compaction with reduction in the size of the macromolecule. For the precursor, the Q-dependent values determined from NSE for $D_{eff}(Q)$ are clearly larger than D_{DLS}. This enhanced mobility is, as previously commented, due to contributions of internal modes that become apparent when exploring the proper length scales by NSE. They become more and more important with increasing Q-value, i. e., reducing the length scale of observation. In the case of the SCNPs, at the lowest Q-value accessible by NSE we find the somehow counterintuitive result of a clearly smaller value of the effective diffusion coefficient than that obtained by DLS. Though the NSE results at 0.03 Å^{-1} present relatively large error bars and the function does not completely decay to 0 within the dynamic window of the instrument, this result is beyond the uncertainties.

As anticipated above, the dynamic structure factor in the NSE window has two contributions: one from the translational diffusion and another one from the relaxation of the internal modes. In general, the translational diffusion coefficient of particles in solution depends on Q and concentration, and can be written as

$$D_{CM}(Q,c) = \frac{D_o H(Q,c)}{S_{CM}(Q,c)}. \tag{7}$$

Here D_o is the self-diffusion coefficient at infinite dilution and $H(Q,c)$ is the hydrodynamic factor. The hydrodynamic factor is not easy to obtain. Some approximations have to be usually made for estimating it. According with some works,[18,51] we have assumed that it is Q-independent: $H(Q,c) \approx H(c)$. Then, for a given concentration the product

$D_oH(Q,c) = D_oH(c)$ is a constant. Taking into account Eq. 7, under this condition the product $D_{CM}(Q,c)S_{CM}(Q,c)$ is the same independently of the Q-value considered. Thus, if we are able to determine it for a particular Q-value, it will be known for other Q-values. We can consider the case $Q \to 0$, that is the situation in DLS. From such experiments we have obtained $D_{DLS}(c) = D_{CM}(Q \approx 0, c)$ for the concentration investigated by NSE. Thus, the diffusion coefficient at any other Q-value can be written as:

$$D_{CM}(Q,c) = \frac{D_{DLS}(c)}{\frac{S_{CM}(Q,c)}{S_{CM}(Q\approx 0,c)}}. \tag{8}$$

The other piece of information needed concerns the structure factor of the centers of mass $S_{CM}(Q,c)$. This has been provided by the SANS measurements. The denominator in Eq. 8 can be obtained by dividing the (smoothed) SANS results shown in Fig. 5(a) by their extrapolated value at $Q \approx 0$. We note that the application of multiplicative factors in the calculation of $S(Q)$ has no effect on this ratio. The such obtained results for $D_{CM}(Q, c{=}25\text{mg/mL})$ are displayed as empty symbols in Fig. 5(b). Errors have been estimated considering the uncertainties in the extrapolation of the structure factor to the Q-value corresponding to DLS and the dispersion of the experimental $S_{CM}(Q)$ data. The diffusion coefficient of the SCNPs shows a weak minimum mirroring the broad maximum of the structure factor. The slowing down of collective diffusion at length scales corresponding to equilibrium inter-particle distances –where the correlations between particles are most pronounced– reflects the well-known deGennes narrowing.[52] Due to this effect, the value of D_{CM} at $Q \approx 0.03\text{Å}^{-1}$ becomes similar, within the uncertainties, to that obtained for D_{eff} from the phenomenological description of the NSE data of the SCNPs [see Fig. 7(c)]. Thus, the dynamic structure factor of the SCNPs at such low-Q values is dominated by the (slowed down) translational diffusion component.

We have also used Eq. 8 to obtain the Q-dependent diffusion coefficient of the precursor[53] [see Figs. 5(b) and 7(c)]. For the linear chains, the translational component is also

sensitively slowed down by the deGennes narrowing. An illustrative magnitude can be built as the difference between the effective diffusion coefficient and the translational diffusion coefficient $\Delta D = D_{eff} - D_{CM}$. This quantity represents to a first approach the importance of the internal degrees of freedom in the decay of the dynamic structure factor. The results, displayed in Fig. 7(d), confirm that in the NSE window the internal dynamics of the SCNPs is strongly suppressed with respect to that of the precursor.

Analyses based on the Zimm model

The chain dynamics of flexible polymers in dilute solution is described[34,37] by the Zimm model.[54] It considers a coarse-grained chain composed by N beads connected by entropic springs of length ℓ. The beads are affected by hydrodynamic interactions mediated by the solvent of viscosity η. In this framework, the resulting Langevin equation can be solved by transforming to the normal ('Rouse') coordinates defined as

$$\vec{X}_p(t) = \frac{1}{N}\sum_{i=1}^{N} \vec{R}_i(t) \cos\left[\frac{p\pi}{N}\left(i - \frac{1}{2}\right)\right]. \tag{9}$$

Here $\vec{R}_i(t)$ is the position vector of the i^{th} bead along the chain and p is the mode number p ($p = 0, ..., N-1$). The zeroth mode corresponds to the center of mass of the chain and the others are associated with internal motions with a 'wavelength' $\ell N/p$. The mode correlators decay exponentially with characteristic times τ_p given by

$$\tau_p^Z = \frac{\eta \overline{R}_e^3}{\sqrt{3\pi} k_B T} p^{-3\nu}. \tag{10}$$

(k_B: Boltzmann constant). Thus, the higher the mode-number, the more localized it is and the faster it decays. The Zimm dynamic structure factor is expressed as:

$$\frac{S_{chain}(Q,t)}{P(Q)} = \frac{1}{N}\exp(-Q^2 D t)\sum_{n,m}^{N} \exp\left(-\frac{1}{6}Q^2 B(n,m,t)\right) \tag{11}$$

in terms of the correlators $B(n,m,t)$:

$$B(n,m,t) = (n-m)^{2\nu}\ell^2 + \frac{4\overline{R}_e^2}{\pi^2} \times \sum_{p=1}^{N-1} \frac{1}{p^{2\nu+1}} \cos\left(\frac{\pi p n}{N}\right) \cos\left(\frac{\pi p m}{N}\right) \left[1 - e^{\left(-\frac{t}{\tau_p}\right)}\right]. \quad (12)$$

The Zimm model was first applied to the results on the reference linear precursor solution. Assuming the length of the beads as the statistical segment deduced for this copolymer (b = 3.27 nm),[17] and taking into account the value of $\overline{R}_e$ obtained from SANS results through Eq. 5 ($\overline{R}_e$ = 19.2 nm), the equivalent chain would consist of N = 20 beads [$\overline{R}_e = bN^{\nu}$, with ν=0.59] (see a compilation of the relevant values of the parameters involved in the fits in Table 2). At the investigated temperature of 298K, η(DMF)=0.82 cP. The Zimm characteristic times [Eq. 10] are represented by the diamonds in Fig. 8 as function of the mode number, p. The dynamic structure factor predicted by the Zimm model [Eqs. 11 and 12] with the Q-dependent values of the diffusion coefficient shown in Figs. 5(b) and 7(c) described well the experimental data only for the lowest Q-value investigated. At higher Qs the model predicts a much more pronounced decay of $S_{chain}(Q,t)$ than that measured (see Fig. S1 of the Supplemental Information, SI). Obviously, approaching local length scales the precursor dynamics strongly deviates from Zimm prediction. Other polymers in solution also shown this kind of behavior (e. g. polyisobutylene[53] or polynorbornenes[55]). To a large extent, the deviations can be attributed to dynamical stiffness.[53,55–57] A straightforward way to take into account this ingredient is restricting the modes contributing to the chain relaxation (considering in Eq. 12 modes up to a given maximum mode number p_{max}). This mode cutoff could be interpreted in terms of virtually rigid subcoils with all internal modes suppressed.[55] As can be appreciated in Fig. 9, the precursor data can be very well described by choosing p_{max}=6. The characteristic times of the considered modes are indicated as filled diamonds in Fig. 8. From the value of p_{max}, the size of the virtually stiff chain sections can be

estimated; their average end-to-end radius would be given by $\overline{r}_e^{stiff} = \overline{R}_e p_{max}^{-\nu}$.[55] In this case, we obtain $\overline{r}_e^{stiff}$= 6.7 nm. This size is about twice the statistical segment, indicating that the dynamic rigidity extends over larger length scales than the static stiffness of the chain. We note in passing that if the deGennes narrowing of the translational diffusion coefficient is not considered, this effect is overestimated.[17]

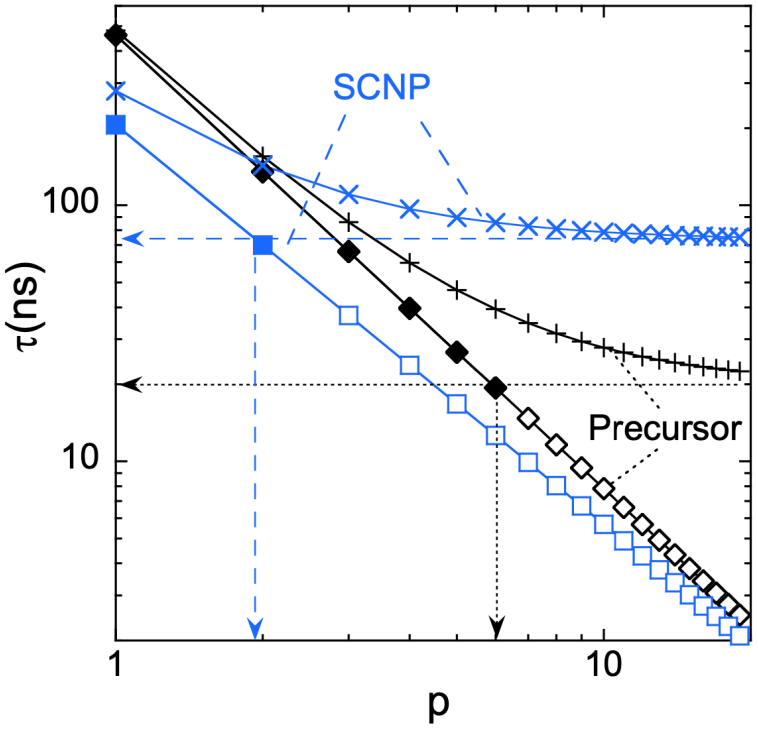

Figure 8: Characteristic times of the Zimm modes as function of the mode number p deduced for the low-M_w precursor (diamonds) and the corresponding SCNPs (squares) in solution. Only modes with $p \leq 6$ (precursor) and $p \leq 2$ (SCNPs) highlighted as filled symbols would substantially contribute. Plusses and crosses represent the characteristic times for the ZIF model for the precursor and the SCNPs respectively. Dotted (dashed) arrows mark the value of τ_i and the location of the crossover from solvent- to internal friction dominated relaxation for the precursor (SCNPs).

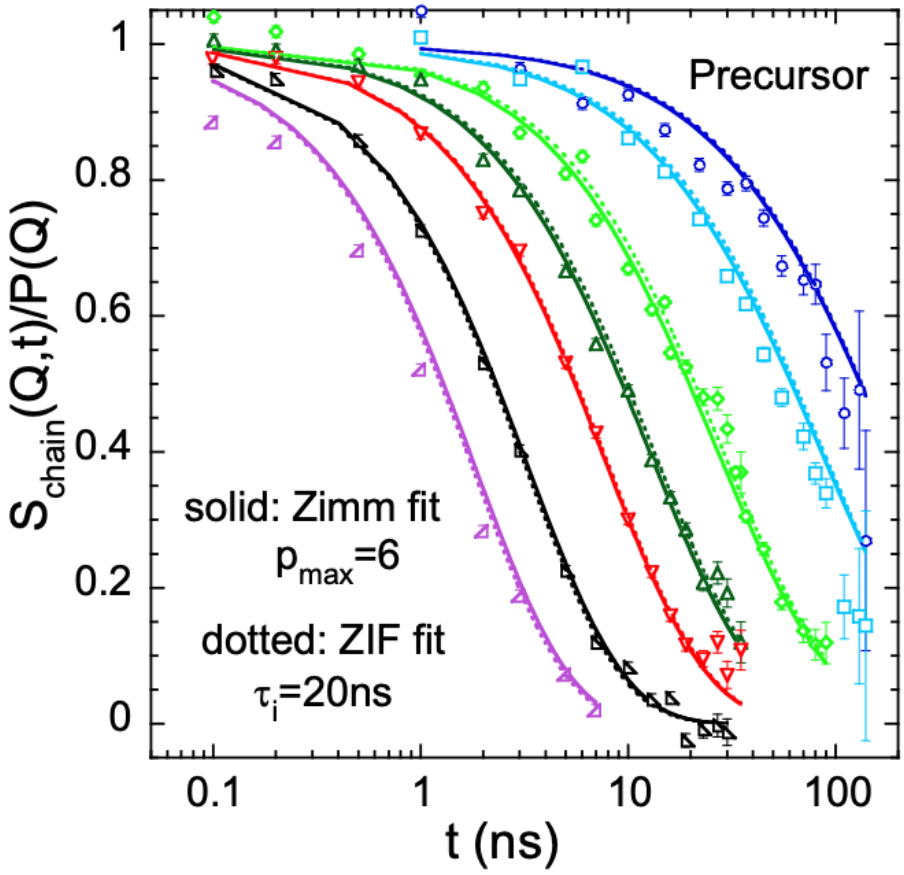

Figure 9: NSE results on the low-M_w precursor solution at different Q-values as specified in Fig. 6, fitted by the Zimm model restricted to the modes corresponding to the longest wavelengths, up to p_{max}=6 (solid line) and Zimm model with internal friction (τ_i=20 ns)(dotted line).

Table 2: Diffusion coefficient measured by DLS at 25 mg/mL and parameters involved in the application of the theoretical approaches used to describe the dynamic structure factor, or derived from them

System	D_{DLS} (Å^2/ns)	$\overline{R}_e$ (nm)	ν	N	ℓ (nm)	τ_1 (ns)	p_{max}	r_e^{stiff} (nm)	τ_i (ns)
low-M_w Precursor	5.77	19.2	0.59	20	3.3	461	6	6.7	20
low-M_w SCNPs	5.85	14.7	0.52	20	3.1	206	2	10.3	73
high-M_w SCNPs	3.38	22.0	0.46	71	3.1	693	4	11.6	120

In the so-called Rouse and Zimm models with internal friction (RIF and ZIF, respectively)[58] the internal friction originated from diverse sources –e. g. internal barriers, side-chain interactions, hindered dihedral rotations, or even hydrogen bonding– is represented by a relaxation time τ_i, which is added to the time of each mode in Eq. 10. The resulting characteristic time for the p^{th}-mode thus becomes $\tau_p^{ZIF} = \tau_p^Z + \tau_i$. The precursor data were analyzed in terms of this approach, considering Eqs. 11 and 12 with $\tau_p = \tau^{ZIF}$. The description obtained by choosing τ_i=20 ns is very good, as can be seen in Fig. 9. It is practically indistinguishable from that obtained by the previous approach. The corresponding spectrum of relaxation times is represented by the plusses in Fig. 8. In the ZIF approach, the drastic effect previously imposed by the mode cutoff p_{max} (equivalent to freeze the modes with $p > p_{max}$, i. e, $\tau^Z_{p>p_{max}} \equiv \infty$) enters in a smoother way. It is represented by a transition from solvent-friction dominated relaxation (low-p values, equivalently long-wavelength modes) to relaxation where internal friction dominates (high-p values, equivalently short-wavelength modes). This crossover occurs when $\tau_p^Z \approx \tau_i$ (see Fig. 8).

Strong internal friction effects leading to deviations from Zimm behavior in the linear precursor chains can be explained, given the chemical nature of the backbone (see Fig. 1). Poly(methyl methacrylate) is a rather rigid polymer. A copolymer of MMA and AEMA units has additional longer side groups scattered along the chain, that are expected to hinder even more its conformational transitions.

We now move to the more complicated systems. The results on the SCNPs solutions are shown in Fig. 10 for the two molecular weights investigated. Only a rather subtle effect of

M_w is observed, despite the large difference in mass (about 5-fold). The interpretation of these data is not as straightforward as for the precursor chains, since the Zimm model and its modified versions are in principle not directly applicable to a SCNP with topology different from that of a linear chain. We note that our nano-particles are half-way between polymeric and 'colloidal' entities. The particle-like nature of the SCNPs has an impact in their center-of-mass diffusion when inter-macromolecular interactions start to be noticeable, as we have previously seen. On the other hand, due to the softness and internal loop structure of the SCNP (see Fig. 3), internal degrees of freedom associated to the relaxation of chain strands and involving flexible domains of the macromolecule are expected to contribute to the decay of the dynamic structure factor. Taking into account these considerations, we can still try to describe the NSE results of the SCNPs under certain assumptions and approximations. First of all, we consider the simultaneous occurrence of independent translational diffusion –characterized by the center-of-mass diffusion D_{CM}– and internal motions. This assumption allows describing the single-chain dynamic structure factor as the product of the corresponding contributions,

$$\frac{S_{chain}(Q,t)}{P(Q)} = \exp(-Q^2 D_{CM} t) S_{int}(Q,t) \tag{13}$$

where $S_{int}(Q,t)$ is the normalized dynamic structure factor corresponding to the internal motions of the macromolecule. Accordingly, we can obtain $S_{int}(Q,t)$ just by simple division of the experimental results by the translational contribution:

$$S_{int}(Q,t) = \exp(Q^2 D_{CM} t) \frac{S_{chain}(Q,t)}{P(Q)} \tag{14}$$

Figure 11 illustrates this deconvolution procedure for the two SCNPs solutions. For the translational component, we use the center-of-mass diffusion coefficient D_{CM} above determined from the SANS and DLS experiments [Eq. 8] represented in Fig. 5(b). In accordance with the much bigger size of the high-M_w-SCNPs, their diffusion coefficient is much smaller

than that of the low-M_w-SCNPs. This yields translational contributions $\exp(-Q^2 D_{CM} t)$ –represented by the lines in Fig. 11– decaying at much longer times. The empty symbols in this figure correspond to the deduced internal modes contribution, $S_{int}(Q,t)$. Since for the high-M_w macromolecules the total dynamic structure factor accessed by NSE is much less affected by the slower diffusion, it mainly reflects the internal degrees of freedom. At high-Q values, $S_{chain}(Q,t)/P(Q)$ almost coincides with $S_{int}(Q,t)$.

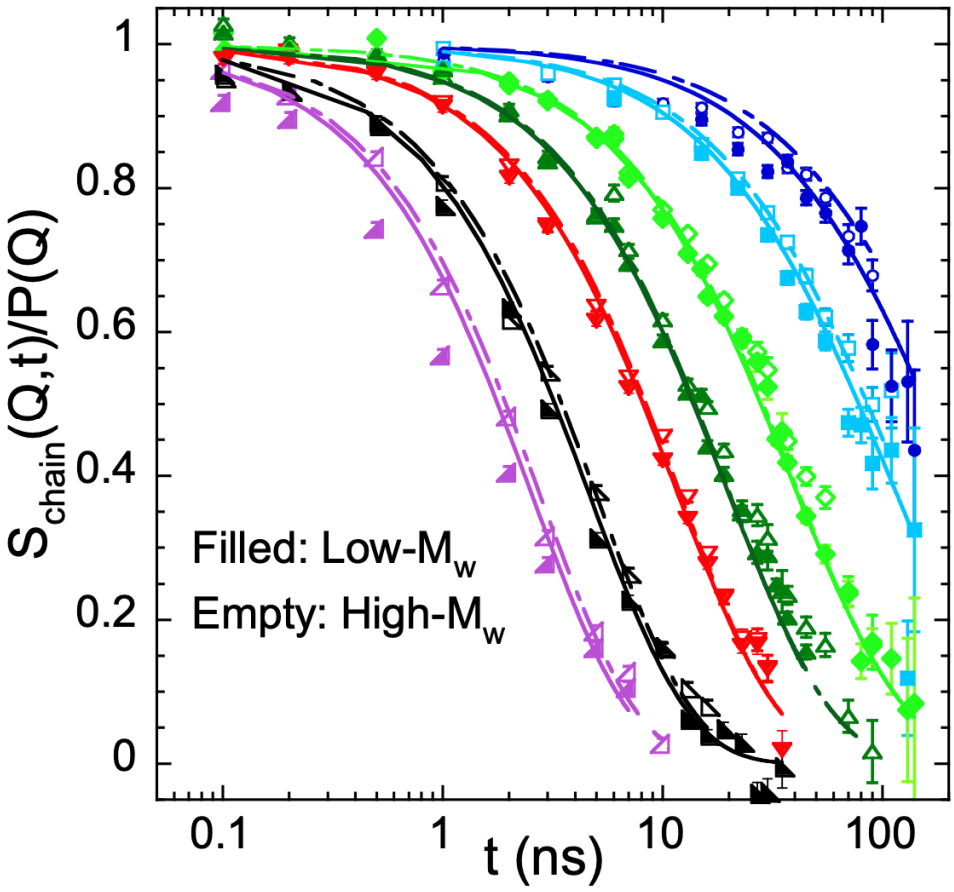

Figure 10: NSE results on the low-M_w (filled symbols) and high-M_w (empty symbols) SCNPs in solution. Different symbols correspond to the different Q-values, as specified in Fig. 6. Lines are fits considering a ZIF-like approach for the internal modes (see the text; solid: low-M_w-SCNPs, τ_i = 73 ns; dashed-dotted: high-M_w-SCNPs),τ_i = 120 ns.

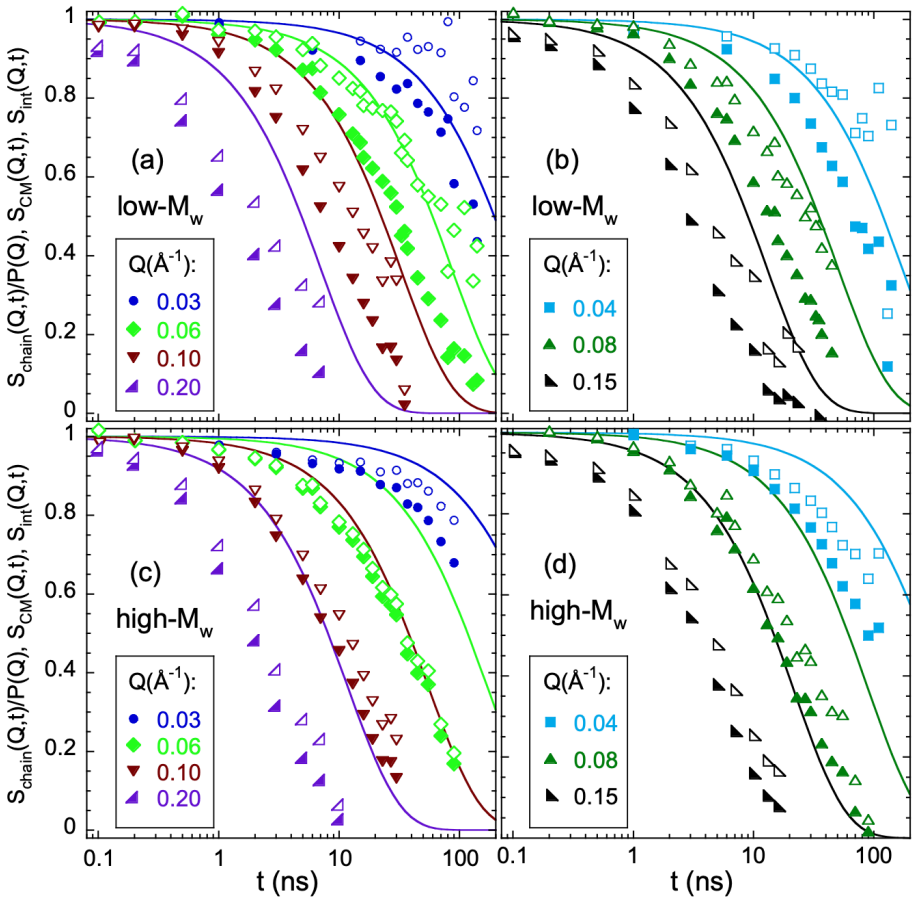

Figure 11: NSE results (filled symbols), center-of-mass diffusion contribution $S_{CM}(Q,t) = \exp(-Q^2 D_{CM} t)$ (solid lines) and internal modes contribution (empty symbols). Different colors correspond to the different Q-values, as specified in the figures. Panels (a) and (b) display results on the low-M_w SCNPs, and (c) and (d) on the high-M_w SCNPs.

The obtained contribution of the internal modes is directly compared for the two molecular weights in Fig. 12. While at high-Q values –local length scales– the results are very similar, this function becomes increasingly slower for the low-M_w SCNPs with decreasing Q. This observation reflects a richer internal dynamics for the bigger macromolecules at larger length scales.

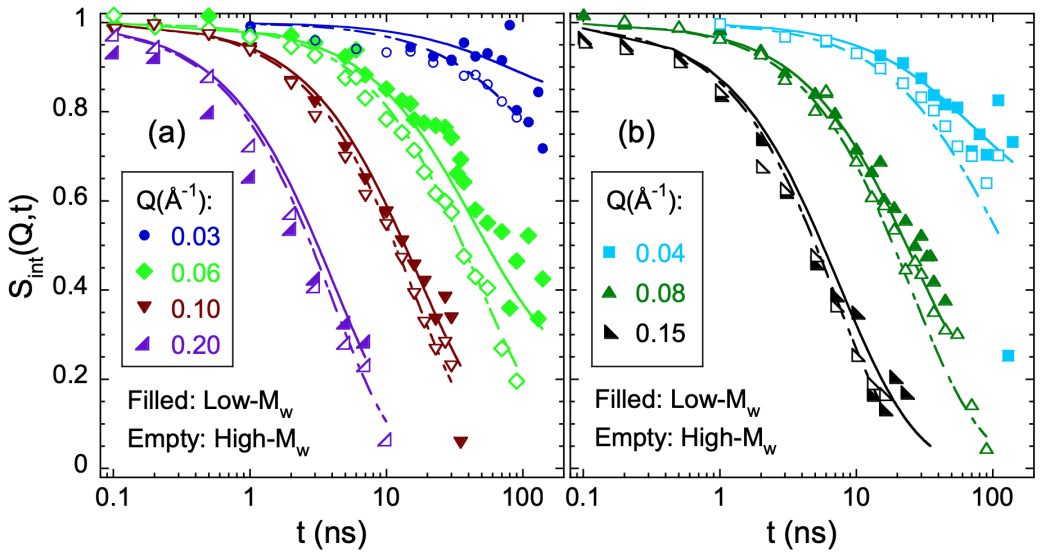

Figure 12: Comparison between the internal modes contributions obtained for the low-M_w (filled symbols) and high-M_w (empty symbols) SCNPs at Q-values 0.03, 0.06, 0.10 and 0.20Å^{-1} (a) and 0.04, 0.08 and 0.15Å^{-1} (b). Lines are descriptions in terms of the Zimm model with limited mode contributions (solid: low-M_w, p_{max}=2; dashed-dotted: high-M_w, p_{max}=4)

In order to be more quantitative in the description of the internal motions, we map the macromolecule to an 'effective' linear chain with the same scaling exponent and dimension as deduced from SANS. The validity of this assumption is supported by a previous work,[17] where MD-simulations provided an independent test of this approach. From the simulation data –directly accessing the monomer coordinates– the normal modes of the effective chain were calculated. The relaxation time of the p^{th}-mode, τ_p, was obtained. For long wavelengths, it was found to be consistent with the Zimm scaling $\tau_p \sim p^{-3\nu}$, with ν the exponent obtained from the fractal regime in the form factor.

We first consider the results for the low-M_w SCNPs. To 'build' the 'effective' chain, the SANS information on the macromolecular conformation (see Tables 1 and 2), $\overline{R}_e$=14.7 nm, ν=0.52, was used. We assumed 20 beads for the mapped chain, in analogy to the case of the precursor chains. This corresponds to a bond length of 3.1 nm. Following analogous steps to those above described for the analysis of the precursor, first, the bare Zimm model was assumed for the internal modes. We thus applied Eq. 12 to calculate the correlators of the equivalent 'effective' chain. The corresponding characteristic times are shown as squares in Fig. 8. They are shorter and follow a weaker mode-number dependence than those of the precursor, due to the smaller dimensions and smaller value of the scaling exponent. The first Zimm mode (p=1) corresponding to the rotational relaxation time amounts to 206 ns for the SCNPs, while in the linear precursor this time is much longer, namely 461 ns. As we could expect from the phenomenological analysis and the failure of the pure Zimm model in accounting for the precursor results, this approach clearly fails also describing the experimental results of the SCNPs.

In the next step, the modified version of the Zimm model using a cut-off for the mode summation was considered for the internal modes. We obtain a satisfactory agreement with p_{max}=2 [see Fig. 12]. The characteristic times of the contributing modes are represented as filled squares in Fig. 8. The internal dynamics of the internally cross-linked macromolecules is extremely hindered –only one 'effective' internal mode, besides the rotational mode, persists

in average. The virtually rigid subcoils would span over about $\overline{r}_e^{stiff} \approx 10$ nm. This constitutes a large fraction of the macromolecule, taking into account its overall size $\overline{R}_e$=14.7 nm. In the final step, the ZIF model was applied for the internal modes. A reasonable description of the data is achieved, as shown in Fig. 10, with τ_i=73 ns. The descriptions achieved by both modified Zimm models are, as in the case of the precursor, nearly indistinguishable among them. (The good quality of the fits can also be appreciated in the semilog-y representation of Fig. S2 in the SI). The p-dependent characteristic times deduced from the ZIF-fit are displayed in Fig. 8. The presence of internal cross-links shifts the crossover from internal-friction dominated relaxation to solvent-friction driven dynamics toward smaller mode-numbers (larger wavelengths). Thus, from this comparative analysis of the dynamics of SCNPs and precursors in terms of similar theoretical approximations, we can deduce a clear impact of the internal cross-linking on the chain dynamics. The rigidity deduced by either models is much more marked in the SCNPs than in the precursor, as reflected by a 1/3 factor in p_{max} and a 3.65 factor in τ_i.

For the high-M_w-SCNPs, the 'effective' chain was built as having the same bead size as that for the low-M_w. Then, given the average end-to-end distance $\overline{R}_e$ = 22 nm and the scaling exponent ν=0.46, the number of segments of the equivalent linear chain was N=71. The corresponding Zimm characteristic times are shown in Fig. 13, together with those calculated for the low-M_w case for comparison. These times are represented as function of the 'wavelength' of the mode, $\ell N/p$. They coincide in the $N/p \rightarrow 1$ limit –corresponding to the segmental time of a single bead ($\tau_N \approx$2 ns). As the 'wavelength' increases, the times corresponding to the high-M_w chain become increasingly faster than those of the low-M_w chain. This is due to the smaller scaling exponent, giving rise to a smoother p-dependence of the time. On the other hand, as consequence of the bigger size of the macromolecules, the lowest p mode numbers correspond to longer 'wavelengths'. Again, as expected also for the high-M_w SCNPs, the bare Zimm model considering all the modes does not reproduce the experimental behavior. As can be seen in Fig. 12, considering the freezing of modes

with $p \geq 5$ the model reproduces well the dynamic structure factor of the internal motions. With p_{max}=4 the rigid subcoils would have an average size of $\overline{r}_e^{stiff} \approx 11.6$ nm, somewhat larger than that deduced for the low-M_w system. This would be consistent with the higher degree of compaction achieved by the internal cross-linking procedure in the bigger macromolecules (smaller value of the scaling exponent). We note that, however, the relative size of these frozen subcoils with respect to the whole chain dimension is much smaller in the high-M_w system, retaining thus some more long-wavelength modes their activity and hence contributing to the decay of the dynamic structure factor at small-Q values.

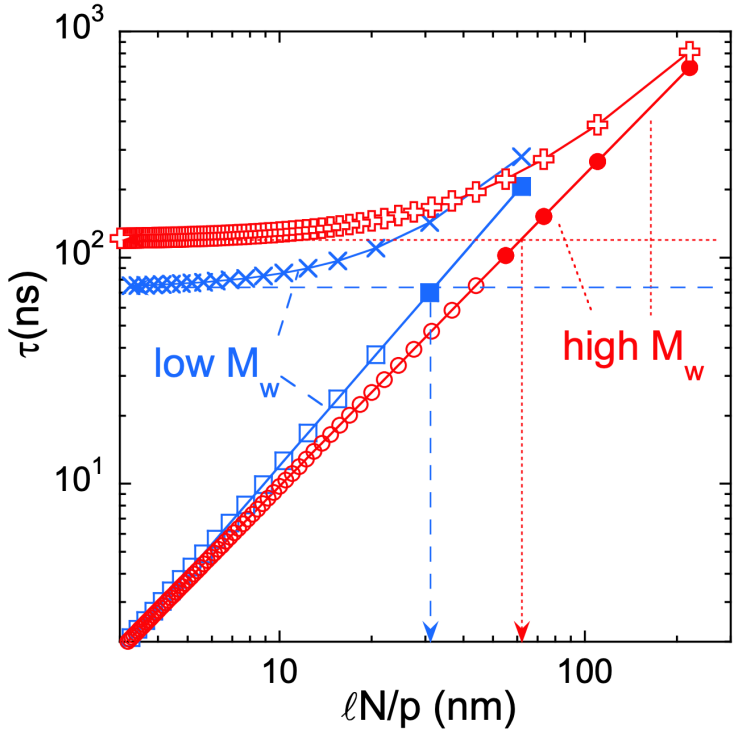

Figure 13: Wavelength-dependence of the characteristic times of the Zimm modes deduced for the 'effective chain' mapping the low-M_w SCNPs (squares) and the high-M_w SCNPs (circles) in solution. Only modes with $p \leq 2$ (low-M_w) and $p \leq 4$ (high-M_w) highlighted as filled symbols would substantially contribute. Crosses and plusses represent the characteristic times for the low-M_w and high-M_w SCNPs respectively.

When the ZIF model is applied, a value of 120 ns for the internal friction time τ_i is obtained for the high-M_w chains (see resulting descriptions in Fig. 10 and also in Fig. S2 of the SI, compared with the other Zimm modified approach in a semilog-y representation). This time is about 50% longer than that found for the low-M_w macromolecules, indicating a higher internal friction associated to the more effective cross-linking synthesis of the high-M_w-SCNPs. We can interpret this longer time as arising from a stronger internal hindrance imposed by a higher density of intramolecular bonds. Figure 13 nicely shows that the wavelength of the modes where the crossover from solvent- to internal friction-dominated dynamics takes place is markedly longer for the bigger chains. Here we may recall the concept of 'domain' introduced above and invoke it as an important ingredient determining the dynamical properties of SCNPs. The high-M_w SCNPs are expected to contain in average larger domains than the low-M_w ones.

We note that the approaches here used to describe the macromolecular dynamics, despite their simplicity, nicely capture the observed phenomenology and provide a rather accurate description of the experimental results (see Figs. 10 and 12 and Fig. S2 in the SI). Further refinements as considering, for instance, partial suppression of the modes could slightly improve the quality of the fits but would increase the complexity of the description by introducing more fitting parameters.

As we have mentioned in the Introduction, in a previous work,[17] we investigated solutions of SCNPs obtained from the same low-M_w precursors as considered here, but applying another synthesis route. This consisted of Cu(II) complexation of AEMA units, exploiting the β-ketoester functional groups in the copolymer precursors. While the crosslinks generated via the Michael synthesis applied in the present study are of covalent nature, those induced by Cu complexation are reversible. SANS experiments on the resulting SCNPs (we shall refer to them as 'Cu-SCNPs') showed a slightly lower degree of compaction (ν=0.54) than that achieved by the Michael procedure applied here. The NSE study on the Cu-SCNPs revealed, despite the different nature of the internal bonds, a rather similar impact on the

internal degrees of freedom. The value of the ZIF characteristic time was τ_i=87 ns, very close –even longer– than that deduced for the irreversible SCNPs here investigated. In terms of the other approach, the maximum mode-number value of the active modes was also p_{max}=2, with an associated frozen characteristic length scale of the same order ($\overline{r}_e^{stiff} \approx$10 nm) as that here deduced for the SCNPs of the same molecular weight. Thus, internal chain dynamics is severely hindered by intramolecular cross-links, even if they are reversible.

The internal compartmentation of SCNPs into domains is thus the source of internal friction, independently of the reversible or irreversible character of the intramolecular bonds. In Ref.[45] the rigidity of the 'domains' identified by MD-simulations was characterized by the relative fluctuation of the domain size. Since domains are composed by merging of several rings within the macromolecule, they are expected to have a strong internal degree of cross-linking and therefore a low deformability. It was found that small domains containing few monomers show the lowest relative fluctuations and are thus weakly deformable. The rigidity of the domains decreases with increasing domain size. Interestingly, it was found that the whole SCNPs have a higher relative deformability than the domains. This would be the result of persistently active long-wavelength modes, that confer enough mobility to deform the macromolecule despite the presence of internal rigid portions of different sizes.

In the Structural Characterization Section we have commented the similar degree of compaction of SCNPs and Intrinsically Disordered Proteins (IDPs), reflected by the closeness of the ν-exponents in both kinds of macromolecules. The analogies between SCNPs and IDPs regarding the topological disorder and the common presence of locally compact, weakly deformable regions (domains) connected by flexible disordered chain segments was discussed in Ref.[45] The similarities between SCNPs and IDPs could also be extensible to dynamical features. As in the case of SCNPs, the interpretation of the dynamic structure factor of biopolymers with a high degree of internal disorder like IDPs is not easy. Therefore, polymer-based theoretical approaches –like the Zimm and ZIF models– have been invoked in recent relevant biophysical investigations on dynamical aspects. For instance, a NSE in-

vestigation of the myelin basic protein (MBP) in D_2O[18] including a ZIF analysis revealed a very high impact of internal friction in the dynamic structure factor of this IDP. The slowing down of MBP motions with respect to a Gaussian polymer behavior was attributed to the fact that the protein is not completely unfolded, but retains a compact core and a folded secondary structure content of 44%. The relevance of internal friction for partially folded molten globules and denaturated states of the protein apomyoglobin –a model system for the investigation of protein folding– was recently studied by NSE in Ref.[59] In that work, the internal friction resulting from transient formation of secondary structure elements in the acid unfolded state was found to be of similar extent to that arising from the presence of α-helices in the molten globule state. Internal friction disappears in fully denaturated apomyoglobin, that adopts an expanded state in the solution. That study thus points to the presence of domains (secondary structure elements) as the main source for internal friction in proteins. We also note that our observation of an increase of the internal friction with increasing compactness of the macromolecule is fully in line with the behavior reported by several authors[60–62] for disordered proteins. It is also worthy of remark that secondary structure is not the only source for internal friction in IDPs, as shown for MBP in Ref.[63] Under fully denaturing conditions, where secondary structure is entirely lost, NSE experiments have evidenced a significant internal friction that would be attributed to the large number of charged amino acid residues and the absence of hydrophobic residues in the macromolecule.

Finally, another very interesting NSE work worth to be commented here is that on denaturated bovine serum albumin (BSA).[64] Chemical denaturation of this protein leads to a very high internal flexibility, translated into a low internal friction ($\tau_i \approx$ amounts to about 3-7% of $\tau_{p=1}$) when disulfide bonds are broken. If these internal bridges remain active, the denaturated protein displays a much stiffer behavior, with an about 10-fold internal friction time. However, in this case, a high impact on the long-wavelength modes is also observed: their amplitudes are strongly suppressed. Contrarily to the case of SCNPs, where domains are predominantly small,[45] a relevant fraction of 'monomers' (amino acids) in denaturated

BSA with intact disulfide bridges belong to large loops containing 45 or 46 amino acids. Thus, the distributions of the domain sizes are very different in both cases, leading to distinct effects in the dynamic properties.

Conclusions

We have investigated the structure and dynamics of irreversible single-chain nano-particles (SCNPs) synthesized via Michael addition in solution. Two molecular weights have been considered. SANS has demonstrated the reduction in size dimensions and decrease of the scaling exponent of the macromolecules upon the creation of internal cross-links. Despite the compaction –that is stronger for the higher molecular weight macromolecules–, the SCNPs exhibit a far from globular topology in good solvent, corroborating earlier findings.[40]

Our study nicely reveals the dual nano-particle / polymer nature of these nano-objects. The interactions with neighboring particles are reflected in a clear peak in the structure factor; at the same time, a high internal mobility is retained by the flexible strands within the macromolecules. This mobility is markedly reduced with respect to the precursor counterparts –the main dynamical signature of internal cross-links.

The NSE results have been analyzed in terms of theoretical approximations based on the Zimm model. Internal friction plays a major role in the dynamics, even for the linear precursor chains. The internal friction clearly increases in the SCNPs, leading to a much slower local relaxation. In larger SCNPs the internal friction is stronger due to the higher density of internal cross-links. However, the persistence of activity of the longest wavelength modes gives rise to a still pronounced relaxation of the dynamic structure factor in the large SCNPs at low-Q values. Playing with the molecular weight and varying the degree of cross-linkers along the chains could thus allow to tune (a) the internal flexibility at long wavelengths and (b) the degree of compartmentation of SCNPs. These measures will help to produce nano-objects with optimized characteristics to be used e. g. as nano-carriers.

The concept of 'domains' –hardly deformable clusters composed of several rings within the macromolecule– can be invoked as the source of the internal friction in SCNPs. The analogies and similarities found between SCNPs and some disordered proteins regarding both, structural and dynamical features are remarkable, suggesting SCNPs as excellent synthetic candidates to mimic certain classes of bio-macromolecules for future investigations. In particular, currently used 'standard' synthesis routes for SCNPs lead to entities that would serve as mimic of bio-macromolecules where weakly deformable compact regions are connected by flexible segments, under the condition that the domains do not span over very large portions of the macromolecule. The domains of these SCNPs could effectively play the role of secondary structure elements in the biological systems. Vice versa, taking inspiration from IDPs,[63] we would expect that charges and hydrophobicity probably will also affect the internal flexibility of SCNPs. Nature could thus be a very useful guide to explore new means for tuning the properties of synthetic SCNPs.

Conflicts of interest

There are no conflicts to declare.

Associated content

Supporting information includes additional NSE plots.

Acknowledgements

The authors gratefully acknowledge the financial support of the Basque Government, code: IT-1175-19 and the Ministerio de Economía y Competitividad code: PGC2018-094548-B-I00 (MCIU/AEI/FEDER, UE). This work is based on experiments performed at KWS-2 and J-NSE (Heinz Maier-Leibnitz Zentrum (MLZ), Garching, Germany), and has been supported

by the European Commission under the 7th Framework Programme through the 'Research Infrastructures' action of the 'Capacities' Programme, NMI3-II Grant Number 283883.

References

(1) Pérez-Baena, I.; Barroso-Bujans, F.; Gasser, U.; Arbe, A.; Moreno, A. J.; Colmenero, J.; Pomposo, J. A. Endowing Single-Chain Polymer Nanoparticles with Enzyme-Mimetic Activity. *ACS Macro Letters* **2013**, *2*, 775–779.

(2) Sánchez-Sánchez, A.; Arbe, A.; Colmenero, J.; Pomposo, J. A. Metallo-Folded Single-Chain Nanoparticles with Catalytic Selectivity. *ACS Macro Letters* **2014**, *3*, 439–443.

(3) Huerta, E.; Stals, P. J. M.; Meijer, E. W.; Palmans, A. R. A. Consequences of Folding a Water-Soluble Polymer Around an Organocatalyst. *Angewandte Chemie International Edition* **2013**, *52*, 2906–2910.

(4) Terashima, T.; Mes, T.; De Greef, T. F. A.; Gillissen, M. A. J.; Besenius, P.; Palmans, A. R. A.; Meijer, E. W. Single-Chain Folding of Polymers for Catalytic Systems in Water. *Journal of the American Chemical Society* **2011**, *133*, 4742–4745.

(5) Altintas, O.; Barner-Kowollik, C. Single-Chain Folding of Synthetic Polymers: A Critical Update. *Macromolecular Rapid Communications* **2016**, *37*, 29–46.

(6) Lyon, C. K.; Prasher, A.; Hanlon, A. M.; Tuten, B. T.; Tooley, C. A.; Frank, P. G.; Berda, E. B. A Brief User's Guide to Single-Chain Nanoparticles. *Polym. Chem.* **2015**, *6*, 181–197.

(7) González-Burgos, M.; Latorre-Sánchez, A.; Pomposo, J. A. Advances in Single Chain Technology. *Chem. Soc. Rev.* **2015**, *44*, 6122–6142.

(8) Mavila, S.; Eivgi, O.; Berkovich, I.; Lemcoff, N. G. Intramolecular Cross-Linking

Methodologies for the Synthesis of Polymer Nanoparticles. *Chemical Reviews* **2016**, *116*, 878–961.

(9) Hanlon, A. M.; Lyon, C. K.; Berda, E. B. What Is Next in Single-Chain Nanoparticles? *Macromolecules* **2016**, *49*, 2–14.

(10) Pomposo, J. A., Ed. *Single-Chain Polymer Nanoparticles: Synthesis, Characterization, Simulations, and Applications*; John Wiley & Sons: Weinheim, Germany, 2017.

(11) Sánchez-Sánchez, A.; Pomposo, J. A. Single-Chain Polymer Nanoparticles via Non-Covalent and Dynamic Covalent Bonds. *Particle & Particle Systems Characterization* **2014**, *31*, 11–23.

(12) Artar, M.; Huerta, E.; Meijer, E. W.; Palmans, A. R. A. *Sequence-Controlled Polymers: Synthesis, Self-Assembly, and Properties*; American Chemical Society, 2014; Chapter 21, pp 313–325.

(13) Sánchez-Sánchez, A.; Pérez-Baena, I.; Pomposo, J. A. Advances in Click Chemistry for Single-Chain Nanoparticle Construction. *Molecules* **2013**, *18*, 3339–3355.

(14) Altintas, O.; Barner-Kowollik, C. Single Chain Folding of Synthetic Polymers by Covalent and Non-Covalent Interactions: Current Status and Future Perspectives. *Macromolecular Rapid Communications* **2012**, *33*, 958–971.

(15) Aiertza, M. K.; Odriozola, I.; Cabañero, G.; Grande, H.-J.; Loinaz, I. Single-Chain Polymer Nanoparticles. *Cellular and Molecular Life Sciences* **2012**, *69*, 337–346.

(16) Moreno, A. J.; Lo Verso, F.; Sánchez-Sánchez, A.; Arbe, A.; Colmenero, J.; Pomposo, J. A. Advantages of Orthogonal Folding of Single Polymer Chains to Soft Nanoparticles. *Macromolecules* **2013**, *46*, 9748–9759.

(17) Arbe, A.; Pomposo, J.; Moreno, A.; LoVerso, F.; Gonzlez-Burgos, M.; Asenjo-Sanz, I.;

Iturrospe, A.; Radulescu, A.; Ivanova, O.; Colmenero, J. Structure and Dynamics of Single-Chain Nano-particles in Solution. *Polymer* **2016**, *105*, 532–544.

(18) Stadler, A. M.; Stingaciu, L.; Radulescu, A.; Holderer, O.; Monkenbusch, M.; Biehl, R.; Richter, D. Internal Nanosecond Dynamics in the Intrinsically Disordered Myelin Basic Protein. *Journal of the American Chemical Society* **2014**, *136*, 6987–6994.

(19) Habchi, J.; Tompa, P.; Longhi, S.; Uversky, V. N. Introducing Protein Intrinsic Disorder. *Chem. Rev.* **2014**, *114*, 6561–6588.

(20) Nguyen, T. K.; Lam, S. J.; Ho, K. K. K.; Kumar, N.; Qiao, G. G.; Egan, S.; Boyer, C.; Wong, E. H. H. Rational Design of Single-Chain Polymeric Nanoparticles that Kill Planktonic and Biofilm Bacteria. *ACS Infectious Diseases* **2017**, *3*, 237–248.

(21) Thanneeru, S.; Nganga, J. K.; Amin, A. S.; Liu, B.; Jin, L.; Angeles-Boza, A. M.; He, J. Enzymatic Photoreduction of Carbon Dioxide using Polymeric Metallofoldamers Containing NickelThiolate Cofactors. *ChemCatChem* **2017**, *9*, 1157–1162.

(22) Chen, J.; Wang, J.; Li, K.; Wang, Y.; Gruebele, M.; Ferguson, A. L.; Zimmerman, S. C. Polymeric Clickase Accelerates the Copper Click Reaction of Small Molecules, Proteins, and Cells. *Journal of the American Chemical Society* **2019**, *141*, 9693–9700.

(23) Sánchez-Sánchez, A.; Akbari, S.; Moreno, A. J.; Verso, F. L.; Arbe, A.; Colmenero, J.; Pomposo, J. A. Design and Preparation of Single-Chain Nanocarriers Mimicking Disordered Proteins for Combined Delivery of Dermal Bioactive Cargos. *Macromolecular Rapid Communications* **2013**, *34*, 1681–1686.

(24) Rubio-Cervilla, J.; Frisch, H.; Barner-Kowollik, C.; Pomposo, J. A. Synthesis of Single-Ring Nanoparticles Mimicking Natural Cyclotides by a Stepwise Folding-Activation-Collapse Process. *Macromolecular Rapid Communications* **2019**, *40*, 1800491.

(25) Liang, J.; Struckhoff, J.; PD, H.; N, R. Preparation and Characterization of Biomimetic β-Lens Crystallins Using Single-Chain Polymeric Nanoparticles. *Langmuir* **2017**, *33*, 7660–7668.

(26) Sánchez-Sánchez, A.; Akbari, S.; Etxeberria, A.; Arbe, A.; Gasser, U.; Moreno, A. J.; Colmenero, J.; Pomposo, J. A. Michael Nanocarriers Mimicking Transient-Binding Disordered Proteins. *ACS Macro Letters* **2013**, *2*, 491–495.

(27) Lindner, P., Zemb, T., Eds. *Neutrons, X-rays and Light: Scattering Methods Applied to Soft Condensed Matter*; North-Holland Delta Series; Elsevier, 2002.

(28) Roe, R.-J. *Methods of X-Ray and Neutron Scattering in Polymer Science*; Oxford University Press: New York, 2000.

(29) Higgins, J. S.; Benoit, H. C. *Polymers and Neutron Scattering*; Oxford University Press: Oxford, 1997.

(30) Gabrys, B., Ed. *Applications of Neutron Scattering to Soft Condensed Matter*; Gordon and Breach Science Publishers: Amsterdam, 2000.

(31) Radulescu, A.; Szekely, N. K.; Appavou, M.-S. KWS-2: Small Angle Scattering Diffractometer. *Journal of Large-Scale Research Facilities* **2015**, *1*, A29.

(32) Mezei, F. *Neutron Spin Echo, Lecture Notes in Physics, Vol. 28*; Springer-Verlag, Heidelberg, 1980.

(33) Ewen, B.; Richter, D. *Neutron Spin Echo Investigations on the Segmental Dynamics of Polymers in Melts, Networks and Solutions*; Adv. Polym. Sci.; Springer Verlag, Berlin Heidelberg, 1997; Vol. 134.

(34) Richter, D.; Monkenbusch, M.; Arbe, A.; Colmenero, J. *Neutron Spin Echo in Polymer Systems*; Adv. Polym. Sci.; Springer Verlag, Berlin Heidelberg New York, 2005; Vol. 174.

(35) Pasini, S.; Holderer, O.; Kozielewski, T.; Richter, D.; Monkenbusch, M. J-NSE-Phoenix, a Neutron Spin-Echo Spectrometer with Optimized Superconducting Precession Coils at the MLZ in Garching. *Review of Scientific Instruments* **2019**, *90*, 043107.

(36) Rubinstein, M.; Colby, R. H. *Polymer Physics*; Oxford: Oxford University Press, 2003.

(37) Doi, M.; Edwards, S. F. *The Theory of Polymer Dynamics*; Clarendon Press: Oxford, 1986.

(38) Hammouda, B. Small-Angle Scattering from Branched Polymers. *Macromolecular Theory and Simulations* **2012**, *21*, 372–381.

(39) Hammouda, B. *SANS from Homogeneous Polymer Mixtures: A Unified Overview*; Advances in Polymer Science; Berlin Heidelberg: Springer Verlag, 1993; Vol. 106; pp 87–133.

(40) Pomposo, J. A.; Pérez-Baena, I.; Lo Verso, F.; Moreno, A. J.; Arbe, A.; Colmenero, J. How Far Are Single-Chain Polymer Nanoparticles in Solution from the Globular State? *ACS Macro Letters* **2014**, *3*, 767–772.

(41) Marsh, J. A.; Forman-Kay, J. D. Sequence Determinants of Compaction in Intrinsically Disordered Proteins. *Biophysical Journal* **2010**, *98*, 2383–2390.

(42) Hofmann, H.; Soranno, A.; Borgia, A.; Gast, K.; Nettels, D.; Schuler, B. Polymer Scaling Laws of Unfolded and Intrinsically Disordered Proteins Quantified with Single-Molecule Spectroscopy. *Proceedings of the National Academy of Sciences* **2012**, *109*, 16155–16160.

(43) Bernado, P.; Svergun, D. I. Structural Analysis of Intrinsically Disordered Proteins by Small-Angle X-Ray Scattering. *Mol. BioSyst.* **2012**, *8*, 151–167.

(44) Smith, W. W.; Ho, P.-Y.; O'Hern, C. S. Calibrated Langevin-Dynamics Simulations of Intrinsically Disordered Proteins. *Phys. Rev. E* **2014**, *90*, 042709.

(45) Moreno, A. J.; Lo Verso, F.; Arbe, A.; Pomposo, J. A.; Colmenero, J. Concentrated Solutions of Single-Chain Nanoparticles: A Simple Model for Intrinsically Disordered Proteins under Crowding Conditions. *The Journal of Physical Chemistry Letters* **2016**, *7*, 838–844.

(46) González-Burgos, M.; Arbe, A.; Moreno, A. J.; Pomposo, J. A.; Radulescu, A.; Colmenero, J. Crowding the Environment of Single-Chain Nanoparticles: A Combined Study by SANS and Simulations. *Macromolecules* **2018**, *51*, 1573–1585.

(47) Oberdisse, J.; González-Burgos, M.; Mendia, A.; Arbe, A.; Moreno, A. J.; Pomposo, J. A.; Radulescu, A.; Colmenero, J. Effect of Molecular Crowding on Conformation and Interactions of Single-Chain Nanoparticles. *Macromolecules* **2019**, *52*, 4295–4305.

(48) Schweizer, K. S.; Curro, J. G. In *Atomistic Modeling of Physical Properties*; Monnerie, L., Suter, U. W., Eds.; Springer Berlin Heidelberg: Berlin, Heidelberg, 1994; pp 319–377.

(49) Pedersen, J. S.; Schurtenberger, P. Static Properties of Polystyrene in Semidilute Solutions: A Comparison of Monte Carlo Simulation and Small-Angle Neutron Scattering Results. *Europhysics Letters (EPL)* **1999**, *45*, 666–672.

(50) Likos, C. N. Effective Interactions in Soft Condensed Matter Physics. *Physics Reports* **2001**, *348*, 267 – 439.

(51) Biehl, R.; Hoffmann, B.; Monkenbusch, M.; Falus, P.; Prévost, S.; Merkel, R.; Richter, D. Direct Observation of Correlated Interdomain Motion in Alcohol Dehydrogenase. *Phys. Rev. Lett.* **2008**, *101*, 138102.

(52) Gennes, P. D. Liquid Dynamics and Inelastic Scattering of Neutrons. *Physica* **1959**, *25*, 825–839.

(53) Arbe, A.; Monkenbusch, M.; Stellbrink, J.; Richter, D.; Farago, B.; Almdal, K.; Faust, R. Origin of Internal Viscosity Effects in Flexible Polymers: A Comparative Neutron Spin-Echo and Light Scattering Study on Poly(dimethylsiloxane) and Polyisobutylene. *Macromolecules* **2001**, *34*, 1281–1290.

(54) Zimm, B. H. Dynamics of Polymer Molecules in Dilute Solution: Viscoelasticity, Flow Birefringence and Dielectric Loss. *The Journal of Chemical Physics* **1956**, *24*, 269–278.

(55) Monkenbusch, M.; Allgaier, J.; Richter, D.; Stellbrink, J.; Fetters, L. J.; Greiner, A. Nonflexible Coils in Solution: A Neutron Spin-Echo Investigation of Alkyl-Substituted Polynorbornenes in Tetrahydrofuran. *Macromolecules* **2006**, *39*, 9473–9479.

(56) Allegra, G.; Ganazzoli, F. Chain Configurations and Dynamics in the Gaussian Approximation. *Advances in Chemical Physics* **2007**, *75*, 265–348.

(57) Richter, D.; Monkenbusch, M.; Allgeier, J.; Arbe, A.; Colmenero, J.; Farago, B.; Bae, Y. C.; Faust, R. From Rouse Dynamics to Local Relaxation: A Neutron Spin Echo Study on Polyisobutylene Melts. *The Journal of Chemical Physics* **1999**, *111*, 6107–6120.

(58) Khatri, B. S.; McLeish, T. C. B. Rouse Model with Internal Friction: A Coarse Grained Framework for Single Biopolymer Dynamics. *Macromolecules* **2007**, *40*, 6770–6777.

(59) Balacescu, L.; Schrader, T. E.; Radulescu, A.; Zolnierczuk, P.; Holderer, O.; Pasini, S.; Fitter, J.; Stadler, A. M. Transition Between Protein-like and Polymer-like Dynamic Behavior: Internal Friction in Unfolded Apomyoglobin Depends on Denaturing Conditions. *Sci Rep* **2020**, *10*, 1570.

(60) Samanta, N.; Chakrabarti, R. Looping Dynamics of a Flexible Chain with Internal Friction at Different Degrees of Compactness. *Physica A: Statistical Mechanics and its Applications* **2015**, *436*, 377 – 386.

(61) Borgia, A.; Zheng, W.; Buholzer, K.; Borgia, M. B.; Schuler, A.; Hofmann, H.; Soranno, A.; Nettels, D.; Gast, K.; Grishaev, A.; Best, R. B.; Schuler, B. Consistent View of Polypeptide Chain Expansion in Chemical Denaturants from Multiple Experimental Methods. *Journal of the American Chemical Society* **2016**, *138*, 11714–11726.

(62) Zheng, W.; Hofmann, H.; Schuler, B.; Best, R. B. Origin of Internal Friction in Disordered Proteins Depends on Solvent Quality. *The Journal of Physical Chemistry B* **2018**, *122*, 11478–11487.

(63) Stingaciu, L. R.; Biehl, R.; Changwoo, D.; Richter, D.; Stadler, A. M. Reduced Internal Friction by Osmolyte Interaction in Intrinsically Disordered Myelin Basic Protein. *The Journal of Physical Chemistry Letters* **2020**, *11*, 292–296.

(64) Ameseder, F.; Radulescu, A.; Holderer, O.; Falus, P.; Richter, D.; Stadler, A. M. Relevance of Internal Friction and Structural Constraints for the Dynamics of Denatured Bovine Serum Albumin. *The Journal of Physical Chemistry Letters* **2018**, *9*, 2469–2473.